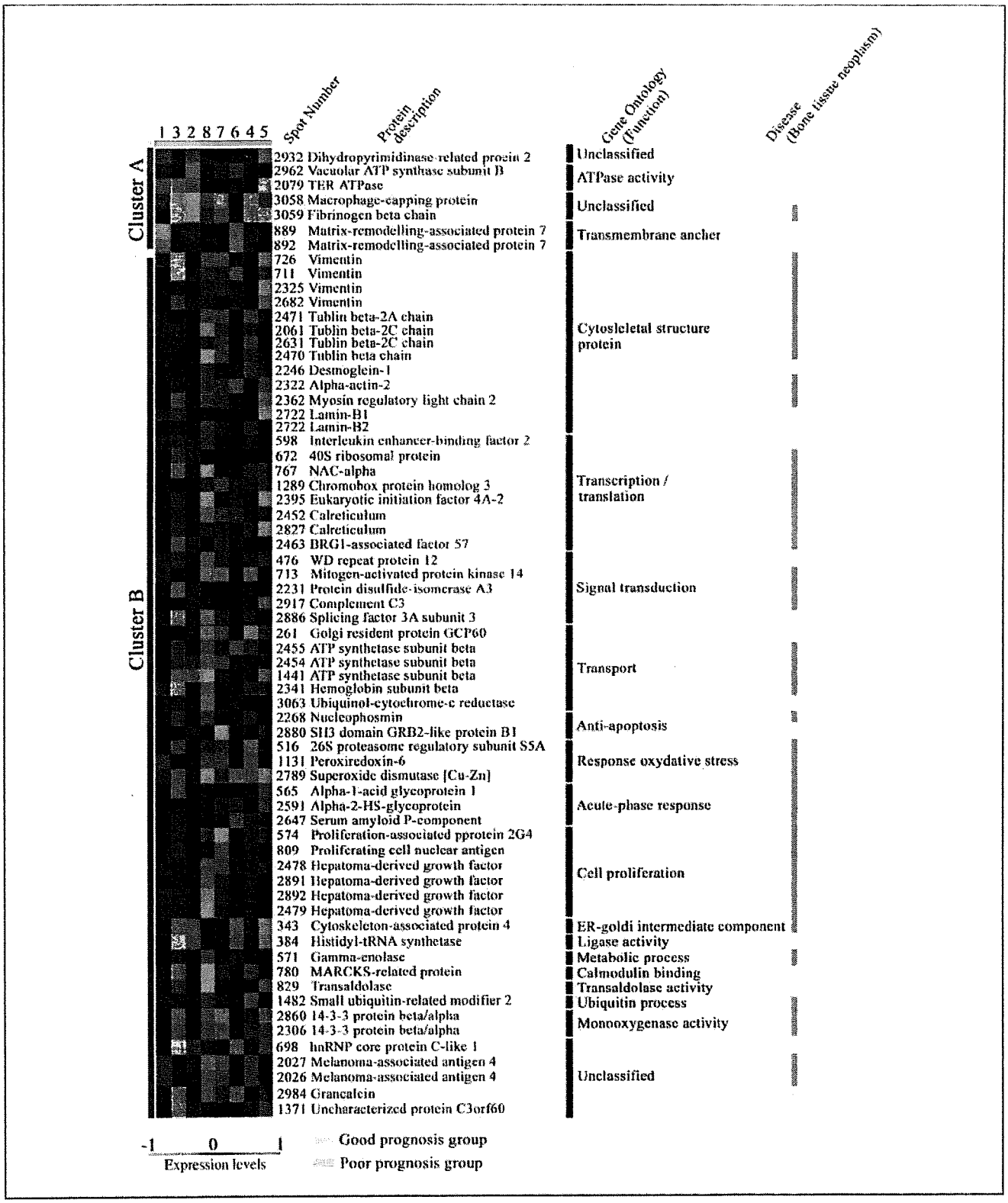

Fig. 2. Hierarchical clustering of the 8 Ewing's sarcoma cases based on the intensity of the 66 protein spots detected. The cases are color-coded as yellow (good prognosis group) or light blue (poor prognosis group). The spot numbers, protein names, Gene Ontology (functional classification), and disease (bone tissue neoplasms; color-coded as red) related proteins are shown (*right*).

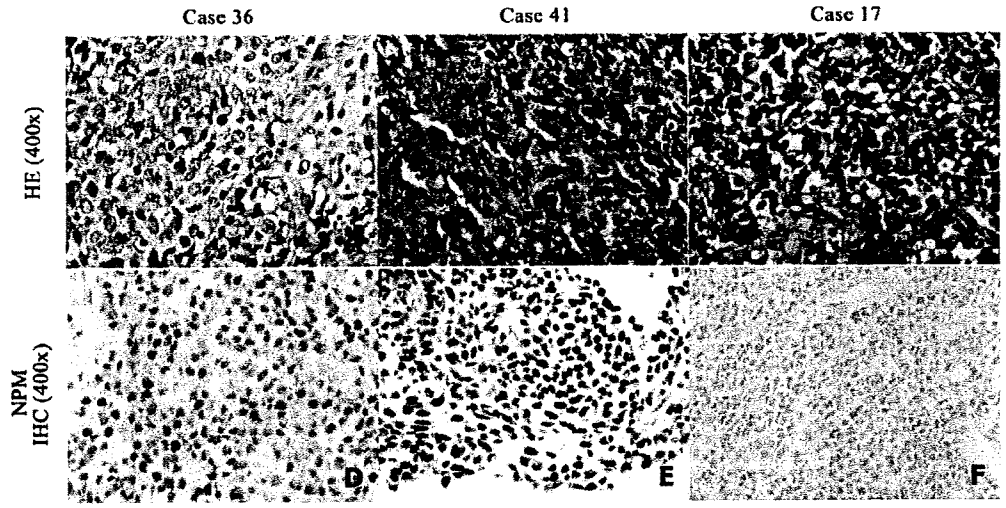

Fig. 3. Nucleophosmin expression was observed in Ewing's sarcoma by immunohistochemistry. *A* to *C*, H&E staining of Ewing's sarcoma cases. Strongly stained nucleophosmin nuclear expression was observed in tumor cells. *D*, dot-like pattern staining. *E*, diffuse-like pattern staining. *F*, not observed stained nucleophosmin nuclear expression. Case numbers correspond to those in Table 2. Magnification, ×400.

that a different patient population was studied, or, finally, the fact that transcriptome and proteome studies cannot uncover entire genome data. These results, therefore, also suggest that studies using proteomic tools are able to reveal unique molecular aspects of Ewing's sarcoma.

Network analysis showed that nucleophosmin is linked with four proteins (c-myc, nuclear factor-κB, Sp1 and p53), which have also been found to be implicated in poor prognosis in Ewing's sarcoma (Supplementary Fig. S1). c-myc has been identified as a potential EWS-ets target gene (40) and as promoting malignant progression of Ewing's sarcoma (41). Activation of nuclear factor-κB was found to contribute to resistance of Ewing's sarcoma cells to apoptosis (42). Coexpression of Sp1 with EWS-ets oncoprotein enhances activation of vascular endothelial growth factor, the expression of which was shown to be a negative predictor of survival in Ewing's sarcoma (43). Aberrations in p53 were found in ~10% of Ewing's sarcoma cases and were associated with shorter survival (44, 45). Taken together, these observations suggest that nucleophosmin can be a single biomarker probably by linking these functionally different proteins. Ewing's sarcoma is characterized by a translocation between the *EWS* gene and a member of the *ETS* family of transcriptional factors (46). The EWS/ETS fusion protein has an altered transcriptional activity and modulates the expression of several downstream target genes (47, 48). The association between the EWS/ETS fusion protein and nucleophosmin should be further investigated.

Nucleophosmin may be used as a novel prognostic biomarker of patients with Ewing's sarcoma. We found that nucleophosmin expression correlated with clinical outcome in 34 Ewing's sarcoma patients. Univariate and multivariate analyses revealed that nucleophosmin expression along with clinical stage (presence of metastases at diagnosis) was an independent prognostic factor in Ewing's sarcoma patients. Furthermore, nucleophosmin expression was also a significant

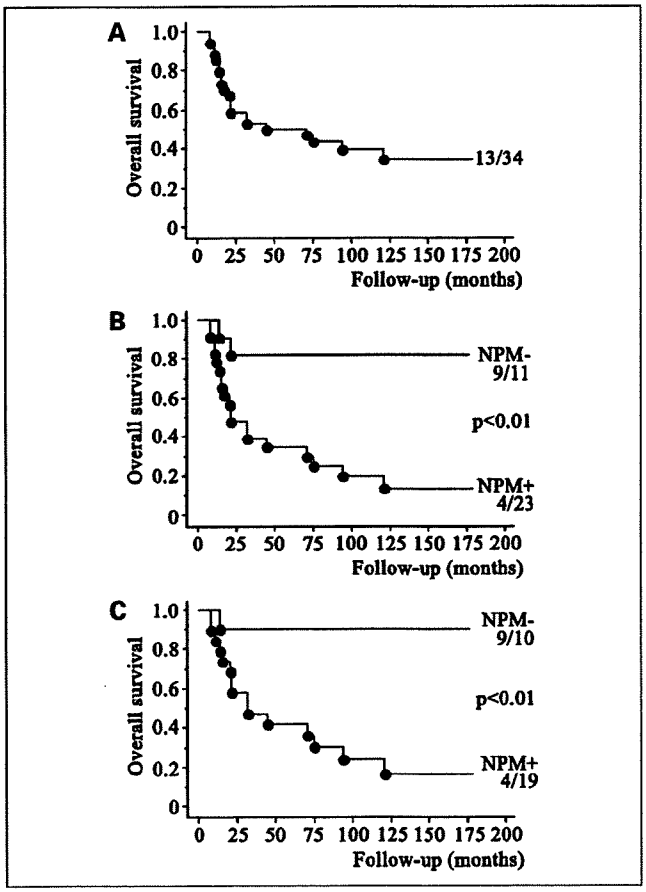

Fig. 4. Kaplan-Meier estimated overall survival curves are illustrated for all patients ($n = 34$; *A*), for all patients based on nucleophosmin positivity (*B*), and for patients with localized disease ($n = 29$) by nucleophosmin positivity (*C*). Statistically significant differences in overall survival periods were observed between the nucleophosmin-positive and nucleophosmin-negative cases both for all cases ($P < 0.01$, log-rank test) and the cases with localized disease ($P < 0.01$, log-rank test).

Table 3. Univariate and multivariate analyses of prognostic factors

Variable	Univariate survival analysis				Multivariate survival analysis	
	No. cases	No. alive	Univariate *P*	Risk ratio (95% confidence interval)	*P*	Relative risk (95% confidence interval)
Age at diagnosis (y)						
<16	9	5	0.3209	1		
≥16	25	8		1.738 (0.583-5.180)		
Sex						
M	22	10	0.5325	1		
F	12	3		0.517 (0.207-1.288)		
Primary site						
Extremity	21	10	0.212	1		
Axial	13	3		1.736 (0.730-4.126)		
Tumor size (cm)*						
<10	16	7	0.0182	1		
≥10	15	2		2.952 (1.202-7.251)		
Clinical stage						
Localized	29	13	<0.01	1	0.0039	1
Metastatic	5	0		5.238 (1.697-16.164)		5.964 (1.773-20.060)
Chemotherapy regimens						
Including IE	17	4	0.0629	1		
Not including IE	17	9		0.425 (0.955-5.791)		
Tumor resectibility						
Resectable	26	12	0.1219	1		
Nonresectable	8	1		2.004 (0.200-1.244)		
Nucleophosmin immunohistochemistry						
Negative	11	9	<0.01	1	0.0063	1
Positive	23	4		7.425 (1.715-32.147)		7.768 (1.783-33.841)

*Tumor size could not be evaluated in 3 Ewing's sarcoma cases.

prognostic factor in patients with localized disease. Applying these findings in a clinical setting poses the next challenge. As the incisional biopsy is a procedure done routinely in establishing the diagnosis in Ewing's sarcoma, the immunohistochemical examination of nucleophosmin expression can be done without any additional invasive examinations.

Although previous reports have suggested a possible association between nucleophosmin and malignancies, the functional role of nucleophosmin in Ewing's sarcoma is still unclear. Nucleophosmin overexpression has been reported to be involved in human tumorigenesis (49, 50). In one study, it led to increased proliferation and inhibition of apoptosis in tumor cells; overexpression of nucleophosmin reduced the percentage of cells in the G_1 phase and increased the S-phase population in the p53-negative cells but induced cell cycle arrest in normal cells. Conducting further basic research on the function of nucleophosmin will pave the way for further understanding of the molecular background of Ewing's sarcoma and, hopefully, for novel diagnostic and therapeutic applications.

In conclusion, global protein expression profiling revealed the proteomic background of Ewing's sarcoma and identified novel associations of several proteins with progression of Ewing's sarcoma. Of the proteins with expression that may have prognostic value, we successfully validated the association of nucleophosmin expression with poor prognosis. The expression of the other proteins may still have prognostic value and further validation studies may prove it. Evaluation of nucleophosmin expression may allow the identification of poor prognosis Ewing's sarcoma patients who may benefit from highly effective treatment in the future.

Disclosure of Potential Conflicts of Interest

No potential conflicts of interest were disclosed.

Acknowledgments

We thank Chizu Kina and Sachiko Miura for excellent technical support in the immunohistochemical study and Yukiko Fujie for excellent technical support in electrophoresis.

References

1. Cotterill SJ, Ahrens S, Paulussen M, et al. Prognostic factors in Ewing's tumor of bone: analysis of 975 patients from the European Intergroup Cooperative Ewing's Sarcoma Study Group. J Clin Oncol 2000; 18:3108–14.
2. Atra A, Whelan JS, Calvagna V, et al. High-dose busulphan/melphalan with autologous stem cell rescue in Ewing's sarcoma. Bone Marrow Transplant 1997;20:843–6.
3. Diaz MA, Vicent MG, Madero L. High-dose busulfan/melphalan as conditioning for autologous PBPC transplantation in pediatric patients with solid tumors. Bone Marrow Transplant 1999;24:1157–9.
4. Bernstein ML, Devidas M, Lafreniere D, et al. Intensive therapy with growth factor support for patients with Ewing tumor metastatic at diagnosis: Pediatric Oncology Group/Children's Cancer Group Phase II Study 9457—a report from the Children's Oncology Group. J Clin Oncol 2006;24:152–9.
5. Engelhardt M, Zeiser R, Ihorst G, Finke J, Muller CI. High-dose chemotherapy and autologous peripheral

blood stem cell transplantation in adult patients with high-risk or advanced Ewing and soft tissue sarcoma. J Cancer Res Clin Oncol 2007;133:1–11.
6. McTiernan A, Driver D, Michelagnoli MP, Kilby AM, Whelan JS. High dose chemotherapy with bone marrow or peripheral stem cell rescue is an effective treatment option for patients with relapsed or progressive Ewing's sarcoma family of tumours. Ann Oncol 2006; 17:1301–5.
7. Grier HE, Krailo MD, Tarbell NJ, et al. Addition of ifosfamide and etoposide to standard chemotherapy for Ewing's sarcoma and primitive neuroectodermal tumor of bone. N Engl J Med 2003;348:694–701.
8. Kolb EA, Kushner BH, Gorlick R, et al. Long-term event-free survival after intensive chemotherapy for Ewing's family of tumors in children and young adults. J Clin Oncol 2003;21:3423–30.
9. Paulussen M, Ahrens S, Burdach S, et al. Primary metastatic (stage IV) Ewing tumor: survival analysis of 171 patients from the EICESS studies. European Intergroup Cooperative Ewing Sarcoma Studies. Ann Oncol 1998;9:275–81.
10. Bacci G, Ferrari S, Bertoni F, et al. Prognostic factors in nonmetastatic Ewing's sarcoma of bone treated with adjuvant chemotherapy: analysis of 359 patients at the Istituto Ortopedico Rizzoli. J Clin Oncol 2000; 18:4–11.
11. Rodriguez-Galindo C, Spunt SL, Pappo AS. Treatment of Ewing sarcoma family of tumors: current status and outlook for the future. Med Pediatr Oncol 2003;40:276–87.
12. Hayes FA, Thompson EI, Meyer WH, et al. Therapy for localized Ewing's sarcoma of bone. J Clin Oncol 1989;7:208–13.
13. Marina NM, Pappo AS, Parham DM, et al. Chemotherapy dose-intensification for pediatric patients with Ewing's family of tumors and desmoplastic small round-cell tumors: a feasibility study at St. Jude Children's Research Hospital. J Clin Oncol 1999;17:180–90.
14. Ohali A, Avigad S, Zaizov R, et al. Prediction of high risk Ewing's sarcoma by gene expression profiling. Oncogene 2004;23:8997–9006.
15. Cheung IY, Feng Y, Danis K, et al. Novel markers of subclinical disease for Ewing family tumors from gene expression profiling. Clin Cancer Res 2007;13: 6978–83.
16. Armengol G, Tarkkanen M, Virolainen M, et al. Recurrent gains of 1q, 8 and 12 in the Ewing family of tumours by comparative genomic hybridization. Br J Cancer 1997;75:1403–9.
17. Maurici D, Perez-Atayde A, Grier HE, Baldini N, Serra M, Fletcher JA. Frequency and implications of chromosome 8 and 12 gains in Ewing sarcoma. Cancer Genet Cytogenet 1998;100:106–10.
18. Hattinger CM, Potschger U, Tarkkanen M, et al. Prognostic impact of chromosomal aberrations in Ewing tumours. Br J Cancer 2002;86:1763–9.
19. Schaefer KL, Eisenacher M, Braun Y, et al. Microarray analysis of Ewing's sarcoma family of tumours reveals characteristic gene expression signatures associated with metastasis and resistance to chemotherapy. Eur J Cancer 2008;44:699–709.
20. Petricoin EF, Ardekani AM, Hitt BA, et al. Use of proteomic patterns in serum to identify ovarian cancer. Lancet 2002;359:572–7.
21. Suehara Y, Kondo T, Fujii K, et al. Proteomic signatures corresponding to histological classification and grading of soft-tissue sarcomas. Proteomics 2006;6: 4402–9.
22. Chen G, Gharib TG, Wang H, et al. Protein profiles associated with survival in lung adenocarcinoma. Proc Natl Acad Sci U S A 2003;100:13537–42.
23. Suehara Y, Kondo T, Seki K, et al. Pfetin as a prognostic biomarker of gastrointestinal stromal tumors revealed by proteomics. Clin Cancer Res 2008;14: 1707–17.
24. Okano T, Kondo T, Fujii K, et al. Proteomic signature corresponding to the response to gefitinib (Iressa, ZD1839), an epidermal growth factor receptor tyrosine kinase inhibitor in lung adenocarcinoma. Clin Cancer Res 2007;13:799–805.
25. Subong EN, Shue MJ, Epstein JI, Briggman JV, Chan PK, Partin AW. Monoclonal antibody to prostate cancer nuclear matrix protein (PRO:4-216) recognizes nucleophosmin/B23. Prostate 1999;39: 298–304.
26. Tanaka M, Sasaki H, Kino I, Sugimura T, Terada M. Genes preferentially expressed in embryo stomach are predominantly expressed in gastric cancer. Cancer Res 1992;52:3372–7.
27. Nozawa Y, Van Belzen N, Van der Made AC, Dinjens WN, Bosman FT. Expression of nucleophosmin/B23 in normal and neoplastic colorectal mucosa. J Pathol 1996;178:48–52.
28. Zhang Y. The ARF-B23 connection: implications for growth control and cancer treatment. Cell Cycle 2004;3:259–62.
29. Tsui KH, Cheng AJ, Chang PL, Pan TL, Yung BY. Association of nucleophosmin/B23 mRNA expression with clinical outcome in patients with bladder carcinoma. Urology 2004;64:839–44.
30. Wolf RE, Enneking WF. The staging and surgery of musculoskeletal neoplasms. Orthop Clin North Am 1996;27:473–81.
31. Shankar AG, Ashley S, Craft AW, Pinkerton CR. Outcome after relapse in an unselected cohort of children and adolescents with Ewing sarcoma. Med Pediatr Oncol 2003;40:141–7.
32. Urano F, Umezawa A, Yabe H, et al. Molecular analysis of Ewing's sarcoma: another fusion gene, EWS-E1AF, available for diagnosis. Cancer Sci 1998;89: 703–11.
33. Kondo T, Hirohashi S. Application of highly sensitive fluorescent dyes (CyDye DIGE Fluor saturation dyes) to laser microdissection and two-dimensional difference gel electrophoresis (2D-DIGE) for cancer proteomics. Nat Protoc 2006;1:2940–56.
34. Kaplan EL, Meier P. Nonparametric estimation from incomplete observations. J Am Stat Assoc 1958;53:1.
35. Cox DR. Regression models and life tables. J R Stat Soc 1972;34:187–220.
36. Obata H, Ueda T, Kawai A, et al. Clinical outcome of patients with Ewing sarcoma family of tumors of bone in Japan: the Japanese Musculoskeletal Oncology Group cooperative study. Cancer 2007;109: 767–75.
37. Yun JP, Miao J, Chen GG, et al. Increased expression of nucleophosmin/B23 in hepatocellular carcinoma and correlation with clinicopathological parameters. Br J Cancer 2007;96:477–84.
38. Bacci G, Ferrari S, Bertoni F, et al. Neoadjuvant chemotherapy for peripheral malignant neuroectodermal tumor of bone: recent experience at the Istituto Rizzoli. J Clin Oncol 2000;18:885–92.
39. Oberlin O, Deley MC, Bui BN, et al. Prognostic factors in localized Ewing's tumours and peripheral neuroectodermal tumours: the third study of the French Society of Paediatric Oncology (EW88 study). Br J Cancer 2001;85:1646–54.
40. Bailly RA, Bosselut R, Zucman J, et al. DNA-binding and transcriptional activation properties of the EWS-FLI-1 fusion protein resulting from the t(11;22) translocation in Ewing sarcoma. Mol Cell Biol 1994;14: 3230–41.
41. Sollazzo MR, Benassi MS, Magagnoli G, et al. Increased c-myc oncogene expression in Ewing's sarcoma: correlation with Ki67 proliferation index. Tumori 1999;85:167–73.
42. Javelaud D, Poupon MF, Wietzerbin J, Besancon F. Inhibition of constitutive NF-κB activity suppresses tumorigenicity of Ewing sarcoma EW7 cells. Int J Cancer 2002;98:193–8.
43. Fuchs B, Inwards CY, Janknecht R. Vascular endothelial growth factor expression is up-regulated by EWS-ETS oncoproteins and Sp1 and may represent an independent predictor of survival in Ewing's sarcoma. Clin Cancer Res 2004;10:1344–53.
44. Abudu A, Mangham DC, Reynolds GM, et al. Overexpression of p53 protein in primary Ewing's sarcoma of bone: relationship to tumour stage, response and prognosis. Br J Cancer 1999;79: 1185–9.
45. de Alava E, Antonescu CR, Panizo A, et al. Prognostic impact of P53 status in Ewing sarcoma. Cancer 2000;89:783–92.
46. Delattre O, Zucman J, Plougastel B, et al. Gene fusion with an ETS DNA-binding domain caused by chromosome translocation in human tumours. Nature 1992;359:162–5.
47. Ladanyi M. EWS-FLI1 and Ewing's sarcoma: recent molecular data and new insights. Cancer Biol Ther 2002;1:330–6.
48. Siligan C, Ban J, Bachmaier R, et al. EWS-FLI1 target genes recovered from Ewing's sarcoma chromatin. Oncogene 2005;24:2512–24.
49. Itahana K, Bhat KP, Jin A, et al. Tumor suppressor ARF degrades B23, a nucleolar protein involved in ribosome biogenesis and cell proliferation. Mol Cell 2003;12:1151–64.
50. Grisendi S, Mecucci C, Falini B, Pandolfi PP. Nucleophosmin and cancer. Nat Rev Cancer 2006; 6:493–505.

DOI 10.1002/prca.200800168 *Proteomics Clin. Appl.* 2009, *3*, 584–596

RESEARCH ARTICLE

Anatomic site-specific proteomic signatures of gastrointestinal stromal tumors

Yoshiyuki Suehara[1, 2, 3], Kazutaka Kikuta[1, 2, 4], Robert Nakayama[2, 4, 5], Kiyonaga Fujii[1], Hitoshi Ichikawa[5], Tatsuhiro Shibata[6], Kunihiko Seki[7]**, Tadashi Hasegawa[7]***, Masahiro Gotoh[8], Naobumi Tochigi[8], Tadakazu Shimoda[7], Yasuhiro Shimada[9], Takeshi Sano[10], Yasuo Beppu[2], Hisashi Kurosawa[3], Setsuo Hirohashi[1], Akira Kawai[2] and Tadashi Kondo[1]*

[1] Proteome Bioinformatics Project, National Cancer Center Research Institute, Tokyo, Japan
[2] Orthopedics Surgery Division, National Cancer Center Hospital, Tokyo, Japan
[3] Department of Orthopedic Surgery, Juntendo University, Tokyo, Japan
[4] Department of Orthopedic Surgery, Keio University, Tokyo, Japan
[5] Cancer Transcriptome Project, National Cancer Center Research Institute, Tokyo, Japan
[6] Cancer Genomics Project, National Cancer Center Research Institute, Tokyo, Japan
[7] Clinical Laboratory Division, National Cancer Center Hospital, Tokyo, Japan
[8] Pathology Division, National Cancer Center Research Institute, Tokyo, Japan
[9] Gastrointestinal Oncology Division, National Cancer Center Hospital, Tokyo, Japan
[10] Gastric Surgery Division, National Cancer Center Hospital, Tokyo, Japan

Received: July 28, 2008
Revised: October 20, 2008
Accepted: November 3, 2008

The gastrointestinal stromal tumor (GIST) is the most common mesenchymal malignancy of the gastrointestinal tract. Its clinical course ranges widely from a curable disorder to a highly malignant disease. Although its clinical and molecular characteristics depend on the anatomic site of origin, the molecular background of GIST arising in different anatomical site has not been studied yet. To investigate the proteomic background of GIST, we examined the proteomic features corresponding to the anatomic site of tumor origin. Comparison of the proteomic profile of gastric (23 cases) and small intestinal (9 cases) GIST by 2-DE revealed 105 protein spots with significantly different intensity ($p < 0.01$) between the two groups. Mass spectrometric study identified 68 distinct proteins for these 105 protein spots, including cancer-associated ones such as prohibitin, pigment epithelium-derived factor, and alpha-actinin 4. The intensity of 37/105 (35.2%) protein spots was significantly concordant with the corresponding mRNA levels ($p < 0.01$). Although both 2-D DIGE and microarray experiments showed significant up-regulation of vimentin expression in small intestinal GIST, Western blotting did not show a significant difference between the two groups. In conclusion, our study demonstrates the proteins specially expressed in GIST depending on their site of origin, as well as the unique advantage offered by use of proteomics to acquire such data. The identified proteins may provide clues to understanding the different characteristics of GIST depending on their site of origin.

Keywords:
2-D DIGE / Anatomic site / Gastrointestinal stromal tumor / Proteomics

Correspondence: Dr. Tadashi Kondo, Proteome Bioinformatics Project, National Cancer Center Research Institute, 5-1-1 Tsukiji, Chuo-ku, Tokyo 104-0045, Japan
E-mail: takondo@ncc.go.jp
Fax: +81-3-3547-5298

Abbreviation: **GIST**, gastrointestinal stromal tumor

* Present address: Department of Structural Biology, Graduate School of Pharmaceutical Sciences, Hokkaido University, Sapporo, Japan
** Present address: Department of Pathology, Japan Railway Tokyo General Hospital, Tokyo, Japan;
*** Present address: Department of Clinical Pathology, Sapporo Medical University School of Medicine, Sapporo, Japan

1 Introduction

The gastrointestinal stromal tumor (GIST) is the most common primary mesenchymal malignancy of the gastrointestinal tract [1, 2]. While the clinical course of GIST ranges widely from a curable disorder to a highly malignant disease, the molecular background of its malignant behavior is largely obscure.

GIST is characterized by the mutation of c-kit and PDGFR, and molecular targeting therapy using imatinib, a tyrosine kinase inhibitor originally developed for the treatment of chronic myeloblastic leukemia, has been proven effective in the treatment of GIST patients. Imatinib has also been shown to suppress the metastasis of GIST post surgery. However, as severe side effects of imatinib treatment have been reported, novel diagnostic modalities to select the patients with poor prognosis before treatment are needed in order to refine current therapeutic strategies. We recently identified pfetin as a novel prognostic biomarker for personalized medicine for GIST patients; by measuring pfetin expression in primary tumor tissues, we can predict the probability for metastasis post surgery [3]. Research avenues to translate these results to clinical application are currently under consideration in our laboratory.

The clinical and molecular characteristics of the GIST tumors depend on the anatomic site of origin. For example, the malignant behavior of GIST has been significantly correlated with the anatomical site of origin; the clinical course of small intestinal GIST is more aggressive than that of gastric ones [4, 5]. Investigation of the molecular background of tumors arising in different anatomical sites through "omics" studies may lead to the development of biomarkers to predict the prognostic biomarker for GIST patients and to novel therapeutic strategies. An array CGH study revealed the presence of site-dependent DNA copy number patterns, including the frequent loss of 1p and 15q in small intestinal and gastric GIST, respectively [6]. A global mRNA expression study resulted in the identification of anatomic site-specific genes, including those involved in muscle contraction and development, modulators for digestive enzymes, cell-cycle regulators, growth factor receptors and mediators of growth factor signaling [7]. Similarly, following mRNA expression studies, connexin 43, a gap junction protein, was extensively studied and was found to be uniquely expressed in small intestinal GIST [8]. Recent reports indicated the presence of mutations in the insulin-like growth factor receptor and BRAF genes [9, 10]. The investigation of genes specific to the anatomic site of origin may provide clues to understanding the molecular background of GIST.

In this report, we conducted a proteomic study to investigate the proteins the expression of which is associated with the site of origin of GIST. The 2-D DIGE detected 105 protein spots that had significantly different intensity between GIST tissues from different anatomic sites. MS identified the proteins corresponding to these 105 protein spots, and their expression levels were compared with their mRNA expression levels as detected by a DNA microarray. To further examine the potential clinical application of our findings, we examined the expression of certain identified proteins, such as vimentin using specific antibodies, and compared the results with those obtained by the proteomic and transcriptomic assays.

2 Materials and methods

2.1 Surgical specimens and clinical information

We examined the tumor tissues from 36 GIST patients who underwent surgery at the National Cancer Center Hospital consecutively from October 1977 to December 2005. All patients underwent resection with curative intent, and were not treated with adjuvant chemotherapy. Pathological diagnosis was based on the WHO classification system for soft-tissue tumors [11, 12], and included the examination of tumor size, presence of necrosis, degree of differentiation, mitotic rate, MIB-1 index, presence of epithelioid cells, and CD34 and CD117 expression. The clinical and pathological data concerning the patients are summarized in Table 1 and Supporting Information Table 1. Consistent with a previous report, c-kit mutations in exon 11 were more frequently observed in the gastric GIST [13-15]. Other factors did not show significant differences between the gastric and small intestinal GIST. This project was approved by the institutional review board of the National Cancer Center.

2.2 2-D DIGE and data analysis

The protein expression profiles were obtained by 2-D DIGE as previously described [3]. In brief, frozen tissues were crushed to powder by CryoPress (Microtech Nichion, Chiba, Japan) under cooling conditions. The frozen powder was then dissolved in a urea lysis buffer containing 6 M urea, 2 M thiourea, 3% CHAPS and 1% Triton X-100. Five micrograms of the protein samples was labeled with CyDye DIGE Fluor saturation dye (GE Healthcare, Uppsala, Sweden). The internal control sample, which was composed of a mixture of small portions of all samples examined in this experiment, was labeled with Cy3 fluorescence dye, while the individual samples were labeled with Cy5 fluorescence dye. These differently labeled protein samples were mixed and co-separated by 2-D PAGE. The first dimension separation was achieved on immobiline dry strip (IPG) gels (24-cm length, *p*I range between 4 and 7, GE Healthcare), and the second separation by SDS-PAGE on 9–16% gradient gels using EttanDalt II (GE Healthcare). Gel images were obtained by scanning the gels with a laser scanner (Typhoon Trio, GE Healthcare) (Supporting Information Fig. 1A). The Cy5 intensity was normalized by the Cy3 intensity in the identical gel for all protein spots using image analysis software (DeCyder version 4.0, GE Healthcare). The data were exported from DeCyder to the Expressionist data-mining package

Table 1. Clinicopathologic features of the training and validation set samples

	Learning set			Validation set
	Stomach	Small intestine		Stomach
	$n = 23$	$n = 9$	P value	$n = 4$
Age	59.9 ± 10.6	65.7 ± 13.5	0.207[a]	66.0 ± 6.0
Gender			0.761[b]	
Male	14	6		2
Female	9	3		2
Histology			0.454[b]	
Spindle	17	6		4
Mixed	4	3		0
Epithelioid	2	0		0
***c-Kit* Mutation**			0.003[b]	
Exon 9	0	4		0
Exon 11	16	3		3
Wild type	7	2		1
Risk classification			0.416[b]	
High	13	4		1
Intermediate	7	2		1
Low	3	3		2
Tumor size (cm)			0.374[b]	
<5cm	5	4		2
5-10cm	8	3		1
>10cm	10	2		1
MIB-1 grading			0.709[b]	
Grade 1	12	5		3
Grade 2	8	2		0
Grade 3	3	2		1

a) Student's *t*-test.
b) Chi-square test.

(GeneData, Basel, Switzerland), to identify the protein spots with statistically different intensity between the sample groups. System reproducibility was verified by running an identical sample three times. Scatter plot analysis revealed that the correlation coefficiency between the independent experiments was more than 0.92 and that the intensity of more than 97% of the protein spots was scattered within a twofold difference range (Supporting Information Fig. 1B). The significance of differences in spot intensity was evaluated using the Wilcoxon test. Hierarchical clustering, principal component analysis (PCA), correlation matrix analysis and spot ranking were performed using the Expressionist software.

2.3 MS protein identification

Protein identification was achieved by MS as previously described [3]. In brief, 100 μg of each protein sample was labeled with Cy5 fluorescence dye and separated by 2-D PAGE. The protein spots were recovered by an automated robot (SpotPiker, GE Healthcare Biosciences, UK). The proteins in the recovered spots were treated with modified trypsin (Promega, Madison, WI) and extracted as trypsin digests, which were then separated by micro-flow HPLC (Paradigm MS4 dual solvent delivery system, Michrom BioResources, Auburn, CA), and subjected to MS/MS (Finnigan LTQ linear IT mass spectrometer, Thermo Electron, San Jose, CA) equipped with a nano-electrospray ion source (AMR, Tokyo, Japan). The MASCOT software (version 2.1, Matrix science, London, UK) was used to search for the mass of the peptide ion peaks against the Swiss-Prot database (*Homo sapiens*, 12 867 sequences in Sprot_47.8 fasta file). Proteins with a MASCOT score of 35 or more were selected for identification. When multiple proteins were identified in a single spot, the proteins with the highest number of peptides were considered as those corresponding to the spot.

2.4 DNA microarray

DNA microarray data were obtained from the same samples and deposited in a public database (Gene Expression Omnibus, accession number GSM202197-202228). The procedures followed for the gene expression study are described in the Gene Expression Omnibus database (http://www.ncbi.nlm.nih.gov/geo/).

2.5 c-kit and PDGFRA mutation studies

The tumor tissues were examined for the mutation status of the c-kit and PDGFRA genes in our previous study [3].

2.6 Western blotting

The expression of vimentin was examined employing a specific antibody. Using 10 μg of each of the protein samples, the samples were separated by SDS-PAGE, transferred onto an NC membrane and incubated with a mouse mAb against vimentin (1:200 dilution, Sigma-Aldrich, Saint Louis, MO) and a HRP-conjugated secondary antibody (1:1000 dilution, GE Healthcare Biosciences). The immune complex was detected by enhanced chemiluminescence (ECL, GE Healthcare) and LAS-3000 (Fuji Film, Tokyo). The relative expression level of vimentin was normalized with that of actin in the same samples using ImageQuant TL software (GE Healthcare).

3 Results

3.1 Overall features of protein expression of GIST tissues

The protein expression profiles of 36 primary GIST were generated employing 2-D DIGE. Altogether, 1411 protein spots were observed in more than 75% of Cy3 images of the internal control sample, and these protein spots were selected to be further examined. Although potentially resulting in loss of information, this trimming process decreased the possibility of irrelevant expression data being studied. The overall features of the proteome were investigated by unsupervised classification methods such as hierarchical clustering analysis (Supporting Information Fig. 1C) and PCA (Supporting Information Fig. 1D). The GIST tissue samples were not clearly separated according to their site of origin based on the intensity of these 1411 protein spots.

3.2 Proteins differentially expressed in gastric and small intestinal GIST

We used 32 of the 36 samples to find the proteins that are differentially expressed in gastric and small intestinal GIST; mRNA expression data were also available for these 32 samples. We then used the remaining four samples to validate the results. We identified 105 protein spots the intensity of which was statistically different ($p < 0.01$) between the gastric (23 cases) and small intestinal (9 cases) GIST. The location of the 105 spots on the 2-D images is shown in Supporting Information Figs. 1A and 2. The GIST samples were separated according to their site of origin based on the intensity of these 105 protein spots using hierarchical clustering (Fig. 1A and Supporting Information Fig. 3) and PCA (Fig. 1B). Correlation matrix analysis revealed that the intensity pattern of the 105 protein spots was similar for GIST tumors of the same site of origin (Fig. 1C). We then examined the four remaining gastric GIST samples, and found that they were clustered with the other gastric GIST samples in hierarchical clustering (Fig. 1D and Supporting Information Fig. 4 for an enlarged image and its heat map) and PCA (Supporting Information Fig. 5).

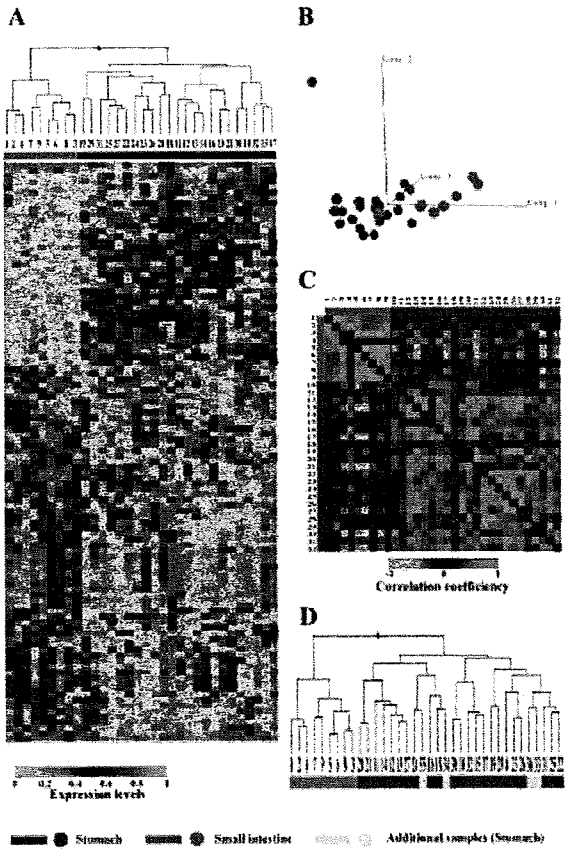

Figure 1. Protein spots with different intensity between the two groups of GIST arising in different anatomic sites. The GIST samples are were grouped based on the intensity of the 105 protein spots by (A) hierarchical clustering and (B) PCA, showing that the samples were grouped according to their anatomic site of origin based on the intensity of 105 protein spots. (C) Correlation matrix demonstrates the sample heterogeneity based on the intensity of the 105 protein spots. (D) An additional four GIST samples of stomach origin were examined by hierarchical clustering to confirm the results. All four samples were fairly classified.

The MS analysis revealed that the 105 protein spots correspond to 72 distinct gene products (Fig. 1A, Supporting Information Figs. 3 and 4, Table 2, and Supporting Information Table 2). The proteins corresponding to all but five protein spots were identified by multiple peptides with significant MASCOT score (Table 2). The 68 or 37 protein spots, the intensity of which was higher or lower in the small intestinal GIST corresponded to 41 and 31 genes respectively. The protein expression level of the peptides recovered from the common preparative gels was not correlated with the MASCOT score.

3.3 Comparison between protein and mRNA expression

The intensity of the 105 identified protein spots was compared with that of the corresponding mRNA expression data generated by a DNA microarray experiment. We calculated the Spearman correlation value for the intensity of each protein spot against the mRNA expression level of their corresponding gene (Figs. 2A–D). Among the 105 protein spots examined, only 37 showed significant correlation in intensity with mRNA expression ($r > 0.449$, $p < 0.01$) (Fig. 2D). Detailed comparison between mRNA and protein expression was performed for nine gene products that generated multiple protein spots. In small intestinal GIST, all protein spots corresponding to annexin A3, glutaminase kidney isoform, and tubulin beta-2 chain showed increased intensity in 2-D DIGE, which corresponded with the mRNA expression of these genes in a statistically significant way (Fig. 2A). Both the spot intensity of 17 of 18 protein spots and mRNA expression of vimentin was higher in the small intestinal GIST (Figs. 1A and 2A, Table 2). Although all of the multiple protein spots for alpha-actinin 4, lamin A/C, pigment epithelium-derived factor and endoplasmin had different intensity between the small intestinal and gastric GIST, their mRNA expression level was not statistically different between the two groups (Fig. 2B). The mRNA expression level of vinculin was statistically higher in the small intestinal than in the gastric GIST (Fig. 2C) although two protein spots for vinculin showed increased intensity in the gastric GIST. The correlation values between the spot intensity and mRNA expression values are summarized in Table 2.

3.4 Concordance between 2-D DIGE, microarray and Western blotting data

Examination of the expression level of vimentin using Western blotting showed that it varied across the samples. Vimentin corresponded to 18 protein spots, all with statistically different intensity between the small intestinal and gastric GIST; in 17 of these spots, the intensity was higher in the small intestinal GIST (Fig. 1A and Table 2). Three bands for vimentin were observed in Western blotting (Fig. 3A). Although the higher intensity of the two bands with lower migration were specific to the small intestinal GIST, only the total intensity of all vimentin bands was taken into account in this study, as the number of samples was small. The sum of the intensity of these three bands was determined and used to compare vimentin with actin expression, actin being the internal control (Fig. 3B). The standardized expression level of vimentin was not statistically significantly different ($p = 0.0749$) between the small intestinal and gastric GIST.

4 Discussion

The anatomic site of origin affects the clinical behavior of a tumor and the molecular characteristics of GIST. Patients with gastric GIST have better prognosis than patients with intestinal GIST [4, 5], and genome-wide global studies have revealed many molecular differences between GIST arising in different sites of origin [6]. By integrating the clinical observations with the molecular aberrations associated with GIST from different sites, we will be able to further understand the molecular background of GIST and to improve the clinical modalities available to GIST patients. Unfortunately, only a limited proteomics study has been reported on GIST to date. Unfortunately, only a limited proteomics study has been reported on GIST to date. As the protein expression level cannot be fully predicted by measuring the corresponding mRNA level and proteins are a functional translation of genes, an expression study at the protein level should also be an effective strategy to establish novel biomarkers. While many lines of evidence have suggested a possible association of genotype aberrations such as exon 11 mutations with the site of origin, genotype aberrations affect the phenotypes only after they are aberrantly translated. With this notion, we performed protein expression profiling in 32 GIST cases with the aim of identifying anatomic-site specific proteins. We found 105 protein isoforms whose expression was statistically different between gastric and small intestinal GIST. This is the first report studying the proteomic signature corresponding to the anatomic site of GIST.

The overall features of the identified proteins were different between the gastric and small intestinal GIST (Figs. 1A and B). These observations suggest that these two types of GIST may have distinct molecular backgrounds, in turn explaining their differing clinical phenotypes. The acquired protein expression data should be validated using additional samples from both gastric and small intestinal GIST. As we believe that most of the identified proteins are not likely to be suitable for clinical use as biomarkers, .we focused our analysis on the proteins the expression of which showed statistically significant differences between the two groups.

We found 105 protein spots with significantly different intensity between the two GIST sample groups (Wilcoxon test p-value less than 0.01) (Fig. 1A). Among them, only 25 protein spots showed more than twofold differences. These observations may suggest two points; first, that GIST arising in different sites may share similar molecular backgrounds

Table 2. A list of identified protein

Spot no.[a]	Accession no.[b]	Identified protein[b]	Wilcoxon test *p* value	Fold difference ratio of means	p*I* (obs)[c]	p*I*[d]	MW (obs) (kDa)[c]	MW (kDa)[d]	Protein score[e]	Peptide matches	Sequence coverage (%)	Symbol	Correlation[f]	Wilcoxon test *p* value (mRNA)[g]	Fold difference ratio of means (mRNA)[g]
780	O94788	Retinal dehydrogenase 2	7.993E-04	6.639	6.0	5.9	60.8	54.8	182	4	5.4	ALDH1A2	0.677	2.652E-04	76.880
1108	P08670	Vimentin	1.925E-03	4.029	5.7	5.1	47.7	53.5	934	29	31.8	VIM	0.644	6.864E-04	1.997
862	P08670	Vimentin	5.439E-04	3.485	5.1	5.1	42.8	53.5	1349	39	54.6	VIM	0.554	6.864E-04	1.997
1022	P08670	Vimentin	1.250E-03	3.439	5.8	5.1	49.0	53.5	895	33	33.5	VIM	0.641	6.864E-04	1.997
1114	P08670	Vimentin	3.347E-03	3.006	5.7	5.1	47.7	53.5	533	13	17.0	VIM	0.615	6.864E-04	1.997
1735	P28161	Glutathione S-transferase Mu 2	1.250E-03	2.951	6.4	6.0	25.5	25.6	444	10	32.3	GSTM2	0.688	8.572E-02	1.300
1021	P08670	Vimentin	5.312E-03	2.810	5.8	5.1	49.0	53.5	789	30	27.1	VIM	0.575	6.864E-04	1.997
951	P08670	Vimentin	3.127E-04	2.801	5.9	5.1	49.7	53.5	1076	31	43.9	VIM	0.758	6.864E-04	1.997
827	P08670	Vimentin	6.443E-03	2.754	5.1	5.1	44.6	53.5	1424	63	52.3	VIM	0.582	6.864E-04	1.997
1158	P08670	Vimentin	5.312E-03	2.660	5.8	5.1	47.0	53.5	639	15	26.9	VIM	0.559	6.864E-04	1.997
854	P07237	Protein disulfide-isomerase precursor	5.031E-04	2.645	4.8	4.8	57.2	57.1	512	11	21.9	P4HB	−0.276	2.578E-01	1.080
1484	P12429	Annexin A3	1.250E-03	2.608	6.7	5.6	33.3	36.2	884	15	45.7	ANXA3	0.898	3.672E-04	2.290
851	P14625	Endoplasmin precursor	4.982E-03	2.593	4.7	4.8	57.2	92.5	274	5	6.2	TRA1	−0.065	3.145E-01	1.088
1574	P12429	Annexin A3	9.282E-04	2.587	6.5	5.6	31.2	36.2	63	1	2.8	ANXA3	−0.261	3.672E-04	2.290
544	P02768	Serum albumin precursor	1.483E-04	2.361	5.4	5.9	75.1	69.4	238	5	7.1	ALB	0.100	6.751E-01	1.182
1272	Q9Y3F4	Serine-threonine kinase receptor-associated protein	5.765E-03	2.317	5.1	5.0	45.0	38.4	250	5	15.4	STRAP	−0.096	6.905E-01	1.051
954	P08670	Vimentin	5.924E-04	2.269	6.0	5.1	49.7	53.5	508	11	21.1	VIM	0.585	6.864E-04	1.997
856	Q9NZW5	MAGUK p55 subfamily member 6	9.697E-03	2.246	5.6	5.8	57.2	61.1	205	4	7.6	MPP6	−0.015	8.572E-02	1.512
865	P08670	Vimentin	9.454E-04	2.241	5.0	5.1	42.8	53.5	805	18	32.7	VIM	0.563	6.864E-04	1.997
309	P02787	Serotransferrin precursor	4.982E-03	2.231	5.8	6.8	48.3	77.1	83	1	1.4	TF	−0.058	7.216E-01	1.036
1109	P08670	Vimentin	9.246E-03	2.204	5.7	5.1	47.7	53.5	738	16	29.2	VIM	0.592	6.864E-04	1.997
948	P08670	Vimentin	1.077E-03	2.171	5.9	5.1	49.7	53.5	866	20	34.0	VIM	0.692	6.864E-04	1.997
1506	P12429	Annexin A3	5.023E-03	2.171	6.7	5.6	32.4	36.2	1076	27	51.2	ANXA3	0.745	3.672E-04	2.290
857	P08670	Vimentin	3.518E-03	2.142	4.8	5.1	57.2	53.5	567	14	21.3	VIM	0.449	6.864E-04	1.997
1854	P00441	Superoxide dismutase [Cu-Zn]	8.213E-04	2.019	7.0	5.7	21.0	15.8	28	1	0.2	SOD1	−0.074	5.025E-01	1.073
457	Q96AY3	FK506 binding protein 10 precursor	2.487E-03	1.984	4.2	5.4	82.3	64.2	214	5	7.6	FKBP10	0.547	7.993E-04	2.336
540	O94925	Glutaminase kidney isoform, mitochondrial precursor	2.444E-04	1.968	5.5	7.9	76.9	73.5	145	3	5.1	GLS	0.418	3.828E-03	5.202
1499	P12429	Annexin A3	1.715E-03	1.964	6.5	5.6	32.1	36.2	128	2	7.5	ANXA3	0.481	3.672E-04	2.290
1043	P36955	Pigment epithelium-derived factor precursor	3.374E-04	1.955	5.7	6.0	49.3	46.3	114	2	5.0	SERPINF1	0.298	5.295E-01	1.480
1830	P28065	Proteasome subunit beta type 9 precursor	2.922E-03	1.899	6.7	4.9	22.5	23.3	130	3	11.4	PSMB9	0.751	2.632E-02	2.389
554	Q14314	Fibroleukin precursor	3.029E-03	1.864	5.3	7.1	76.9	50.2	92	2	4.1	FGL2	−0.002	5.295E-01	1.062
481	P02545	Lamin A/C	5.121E-03	1.817	5.7	6.6	82.3	74.1	1277	22	34.5	LMNA	0.193	6.448E-01	1.003
812	P00352	Retinal dehydrogenase 1	1.790E-03	1.809	5.5	6.3	57.2	54.7	320	8	11.6	ALDH1A1	0.577	2.919E-03	11.300
63	P18206	Vinculin	3.670E-03	1.805	4.1	5.5	114.1	123.7	90	2	1.5	VCL	−0.348	2.922E-03	1.770

Table 2. Continued

Spot no.[a]	Accession no.[b]	Identified protein[b]	Wilcoxon test *p* value	Fold difference ratio of means	*p*I (obs)[c]	*p*I[d]	MW (obs) (kDa)[c]	MW (kDa)[d]	Protein score[e]	Peptide matches	Sequence coverage (%)	Symbol	Correlation[f]	Wilcoxon test *p* value (mRNA)[g]	Fold difference ratio of means (mRNA)[g]
1723	P04632	Calpain small subunit 1	1.247E-03	1.804	6.9	5.1	26.5	28.3	91	2	10.4	CAPNS1	0.224	1.021E-01	1.122
1253	P09471	Guanine nucleotide-binding protein G(o), alpha subunit 1	4.371E-03	1.799	5.8	5.3	45.0	39.9	213	4	11.6	GNAO1	0.567	1.688E-02	2.433
1194	Q13813	Spectrin alpha chain, brain	7.582E-03	1.793	4.0	5.2	90.7	284.5	178	3	1.2	SPTAN1	–0.201	4.258E-01	1.094
555	O94925	Glutaminase kidney isoform, mitochondrial precursor	7.304E-03	1.751	5.3	7.9	76.9	73.5	169	4	6.0	GLS	0.320	3.828E-03	5.202
768	P08670	Vimentin	1.670E-03	1.728	5.2	5.1	50.0	53.5	1045	29	41.7	VIM	0.360	6.864E-04	1.997
900	P68371	Tubulin beta-2 chain	1.719E-03	1.722	5.0	4.8	53.6	49.8	481	13	18.4	TUBB2	0.469	4.885E-02	1.221
977	P68363	Tubulin alpha-ubiquitous chain	2.418E-03	1.698	6.2	5.1	49.3	59.5	299	5	8.1	TUBA6	0.184	9.666E-01	1.000
551	P38646	Stress-70 protein, mitochondrial precursor	3.256E-03	1.692	5.6	5.9	46.7	73.7	1312	31	32.3	HSPA9B	–0.490	6.864E-04	1.353
55	P18206	Vinculin	7.252E-03	1.679	6.1	5.5	35.1	123.7	891	14	13	VCL	0.000	2.922E-03	1.770
771	Q9UJU6	Drebrin-like protein	8.610E-04	1.673	5.1	5.0	50.0	48.2	260	5	12.8	DBNL	0.325	7.835E-02	1.205
1361	P51858	Hepatoma-derived growth factor	2.360E-03	1.673	6.6	4.7	35.4	26.8	76	2	7.9	HDGF	0.006	9.332E-01	1.108
830	P07437	Tubulin beta-2 chain	8.828E-03	1.660	5.1	4.8	43.7	49.7	419	8	16	TUBB	0.042	1.938E-01	1.143
592	Q16555	Dihydropyrimidinase-related protein 2	3.123E-03	1.643	5.3	6.0	73.3	62.3	260	5	10.7	DPYSL2	0.486	8.278E-03	1.370
1203	P62736	Actin, aortic smooth muscle	8.382E-03	1.643	4.2	5.2	90.9	42.0	170	3	8.5	ACTA2	–0.519	2.922E-03	2.361
1689	P02743	Serum amyloid P-component precursor	7.763E-03	1.629	6.4	6.1	28.0	25.4	209	3	15.7	APCS	–0.075	1.000E+00	1.100
213	O43707	Alpha-actinin 4	3.818E-03	1.626	4.4	5.3	114.1	104.9	657	12	14.7	ACTN4	0.113	1.210E-01	1.219
552	O94925	Glutaminase kidney isoform, mitochondrial precursor	9.016E-03	1.618	5.2	7.9	76.9	73.5	190	4	6.3	GLS	0.554	3.828E-03	5.202
842	P68371	Tubulin beta-2 chain	3.667E-04	1.615	5.0	4.8	59.0	49.8	781	26	33.7	TUBB2	0.479	4.885E-02	1.221
1078	P08670	Vimentin	8.668E-03	1.615	5.8	5.1	48.3	53.5	698	16	25.4	VIM	0.555	6.864E-04	1.997
1826	P22352	Plasma glutathione peroxidase precursor	8.586E-03	1.613	6.8	8.2	22.0	25.5	119	3	14.6	GPX3	0.112	5.858E-01	1.252
765	Q02818	Nucleobindin 1 precursor	5.670E-03	1.612	5.1	5.1	50.0	53.9	441	7	15.2	NUCB1	0.050	3.350E-01	1.071
217	O43707	Alpha-actinin 4	5.662E-03	1.611	4.3	5.3	114.1	104.9	744	13	15.9	ACTN4	0.287	1.210E-01	1.219
535	O94925	Glutaminase kidney isoform, mitochondrial precursor (EC 3.5.1.2) (GLS)	2.374E-03	1.608	5.5	7.9	47.0	73.5	199	4	6.6	GLS	0.231	3.828E-03	5.202
1104	O75874	Isocitrate dehydrogenase [NADP] cytoplasmic	1.151E-04	1.607	5.8	6.5	47.7	46.7	468	10	20.5	IDH1	0.663	8.272E-03	1.392
832	P68371	Tubulin beta-2 chain	3.649E-04	1.605	4.9	4.8	59.0	49.8	729	19	36.9	TUBB2	0.470	4.885E-02	1.221
860	P14625	Endoplasmin precursor	3.847E-03	1.603	4.9	5.1	57.2	53.5	771	27	30.3	TRA1	–0.010	3.145E-01	1.088
1598	Q06323	Proteasome activator complex subunit 1	6.443E-03	1.600	4.2	5.8	89.8	28.7	260	6	23.3	PSME1	0.882	2.547E-03	2.054
918	P68371	Tubulin beta-2 chain	1.790E-03	1.598	5.0	4.8	53.6	49.8	850	21	48.3	TUBB2	0.487	4.885E-02	1.221
212	O43707	Alpha-actinin 4	7.774E-03	1.590	4.3	5.3	114.1	104.9	342	7	7.7	ACTN4	0.176	1.210E-01	1.219
488	P02545	Lamin A/C	3.347E-03	1.579	5.8	6.6	82.3	74.1	914	15	22.1	LMNA	0.254	6.448E-01	1.003
1440	P07195	L-lactate dehydrogenase B chain	2.930E-03	1.572	4.1	5.7	92.1	36.5	200	3	8.7	LDHB	0.077	1.112E-01	1.084

Table 2. Continued

Spot no.[a]	Accession no.[b]	Identified protein[b]	Wilcoxon test p value	Fold difference ratio of means	pI (obs)[c]	pI[d]	MW (obs) (kDa)[c]	MW (kDa)[d]	Protein score[e]	Peptide matches	Sequence coverage (%)	Symbol	Correlation[f]	Wilcoxon test p value (mRNA)[g]	Fold difference ratio of means (mRNA)[g]
1289	Q96C86	Scavenger mRNA decapping enzyme DcpS	1.173E-03	1.569	6.0	5.8	44.3	38.7	190	3	11.3	DCPS	0.404	5.878E-04	1.550
1388	Q15181	Inorganic pyrophosphatase	4.371E-03	1.559	4.1	5.5	92.5	32.7	78	2	6.6	PPA1	0.395	1.618E-04	2.140
655	P08670	Vimentin	9.354E-03	1.559	5.2	5.1	53.6	53.5	1206	42	41.7	VIM	0.431	6.864E-04	1.997
455	P11142	Heat shock cognate 71 kDa protein	3.080E-03	1.554	4.3	5.4	82.3	70.9	155	3	4.8	HSPA8	0.333	5.295E-01	1.024
825	P08670	Vimentin	4.982E-03	1.549	4.9	5.1	59.0	53.5	748	16	30.5	VIM	0.257	6.864E-04	1.997
1896	P09382	Galectin-1	9.222E-03	1.535	6.4	5.3	17.9	14.6	108	2	13.4	LGALS1	0.681	3.611E-02	1.326
809	Q96KP4	Cytosolic nonspecific dipeptidase	7.309E-03	1.534	5.0	5.7	43.3	52.9	70	2	4.4	CNDP2	0.033	6.516E-02	1.259
650	P31948	Stress-induced-phosphoprotein 1	7.304E-03	1.527	5.8	6.4	66.1	62.6	326	8	10.5	STIP1	–0.128	5.858E-01	1.094
352	P08238	Heat shock protein HSP 90-beta	6.620E-03	1.521	4.2	5.0	91.2	83.1	568	12	16.0	HSPCB	–0.059	6.443E-03	1.306
426	Q08493	cAMP-specific 3′,5′-cyclic phosphodiesterase 4C	2.922E-03	1.510	4.1	5.1	85.8	79.9	443	9	12.1	PDE4C	–0.193	2.947E-01	1.122
1828	P61019	Ras-related protein Rab-2A	3.579E-03	1.504	5.3	6.1	90.3	23.5	224	3	19.3	RAB2	–0.226	7.692E-01	1.044
666	P61978	Heterogeneous nuclear ribonucleoprotein K	4.215E-03	1.503	5.5	5.4	66.1	51.0	209	6	7.8	HNRPK	–0.088	9.364E-02	1.083
1604	Q9Y696	Chloride intracellular channel protein 4	1.247E-03	1.502	6.6	5.5	30.3	28.8	119	2	9.1	CLIC4	0.798	4.304E-04	1.458
1055	P31930	Ubiquinol-cytochrome-c reductase complex core protein I	2.638E-03	1.500	5.4	5.9	48.0	52.6	173	3	6.0	UQCRC1	–0.210	8.278E-03	1.384
505	P02545	Lamin A/C	6.126E-04	1.499	6.0	6.6	80.5	74.1	1363	27	33.9	LMNA	0.090	6.448E-01	1.003
1592	P35232	Prohibitin	5.858E-04	1.492	6.4	5.6	30.6	29.8	203	4	21.7	PHB	–0.226	4.982E-03	1.241
1512	P09493	Tropomyosin 1 alpha chain	6.096E-03	1.481	4.1	4.7	90.7	32.7	145	3	9.2	TPM1	0.547	5.574E-01	1.158
983	P36957	Dihydrolipoyllysine-residue succinyltransferase component	4.982E-03	1.479	6.0	9.0	49.0	48.6	203	4	9.5	GPR18	–0.165	5.574E-01	1.207
794	P08670	Vimentin	2.298E-03	1.478	5.0	5.1	50.0	53.5	1097	26	41.7	VIM	0.355	6.864E-04	1.997
1761	P60174	Triosephosphate isomerase	2.479E-03	1.463	6.9	6.5	24.5	26.5	229	4	15.3	TPI1	0.054	1.313E-01	1.289
494	P02545	Lamin A/C	2.919E-03	1.462	5.9	6.6	80.5	74.1	1508	23	32.7	LMNA	0.337	6.448E-01	1.003
1460	P40925	Malate dehydrogenase, cytoplasmic (EC 1.1.1.37)	7.720E-03	1.459	5.6	6.9	91.6	36.3	67	1	3	MDH1	0.241	9.360E-03	1.324
567	P08107	Heat shock 70 kDa protein 1	4.760E-03	1.439	5.6	5.5	46.0	70.1	1284	29	30.6	HSPA1A	0.507	2.406E-01	1.088
686	P50990	T-complex protein 1, theta subunit	2.935E-03	1.425	5.7	5.4	45.0	59.5	313	6	11.3	TCP1	0.216	7.692E-01	1.049
752	P48643	T-complex protein 1	4.494E-03	1.414	5.6	5.5	62.5	59.7	315	6	10.4	CCT5	–0.028	7.060E-01	1.079
1263	P00738	Haptoglobin precursor	6.932E-03	1.405	5.4	6.1	45.0	45.2	91	2	4.7	HP	–0.083	1.366E-01	1.702
1057	P36955	Pigment epithelium-derived factor precursor	9.013E-03	1.403	5.9	6.0	48.3	46.3	167	3	7.7	SERPINF1	0.322	5.295E-01	1.480
1510	P60900	Proteasome subunit alpha type 6	4.779E-03	1.388	5.6	6.3	91.2	27.4	74	1	5.3	PSMA6	0.491	1.913E-04	2.227
1555	P08758	Annexin A5	7.576E-03	1.374	6.1	4.9	31.5	35.8	96	2	5.3	ANXA5	–0.009	7.150E-02	1.161
730	P30153	Serine/threonine protein phosphatase 2A	6.113E-03	1.342	5.0	5.0	64.3	65.1	299	6	11.4	PPP2R1A	0.322	8.572E-02	1.226
1564	Q13011	Delta3,5-delta2,4-dienoyl-CoA isomerase	6.986E-03	1.341	6.4	6.6	31.5	36.0	86	2	5.8	ECH1	0.179	7.993E-04	1.606
1096	P61163	Alpha-centractin	8.661E-03	1.340	5.7	6.2	48.0	42.6	204	4	8.5	ACTR1A	–0.024	1.541E-01	1.179
497	P02545	Lamin A/C	7.441E-03	1.336	5.9	6.6	78.7	74.1	1492	28	36.0	LMNA	0.093	6.448E-01	1.003

Table 2. Continued

Spot no.[a]	Accession no.[b]	Identified protein[b]	Wilcoxon test *p* value	Fold difference ratio of means	p*I* (obs)[c]	p*I*[d]	MW (obs) (kDa)[c]	MW (kDa)[d]	Protein score[e]	Peptide matches	Sequence coverage (%)	Symbol	Correlation[f]	Wilcoxon test *p* value (mRNA)[g]	Fold difference ratio of means (mRNA)[g]
1559	P06753	Tropomyosin alpha 3 chain	6.859E-03	1.320	6.7	4.7	31.5	32.8	167	3	11.6	TPM3	0.393	7.692E-01	1.093
1565	Q96GD0	Pyridoxal phosphate phosphatase	8.278E-03	1.316	5.5	6.1	90.3	31.7	201	4	17.2	PDXP	−0.047	1.313E-01	1.322
1153	Q9BT78	COP9 signalosome complex subunit 4	4.364E-03	1.292	5.7	5.6	47.0	46.3	276	5	8.9	COPS4	0.157	1.000E+00	1.013
1807	Q06830	Peroxiredoxin 1	8.767E-03	1.239	5.0	8.3	92.1	22.1	80	2	9.5	PRDX1	−0.195	3.334E-05	2.010
1849	P32119	Peroxiredoxin 2	5.797E-03	1.218	6.4	5.7	21.5	21.8	96	2	9.6	PRDX2	−0.129	5.295E-01	1.112
237	P13639	Elongation factor 2	8.272E-03	1.216	4.7	6.4	114.1	95.2	200	4	4.2	EEF2	0.511	1.424E-01	1.194
1816	P30048	Thioredoxin-dependent peroxide reductase	9.202E-03	1.209	6.1	7.7	23.0	27.7	165	3	14.5	PRDX3	−0.121	3.145E-01	1.086

a) Spot numbers refer to those in Fig. 1A and Supporting Information Fig. 1.
b) Accession numbers of proteins were derived from Swiss-Prot and NCBI nonredundant databases.
c) Observed isoelectric point and molecular weight calculated according to location on the 2-D gel.
d) Theoretical isoelectric point and molecular weight obtained from Swiss-Prot and the ExPASy database (http://au.expasy.org).
e) MASCOT score for the identified proteins based on the peptide ions score ($p < 0.05$) (http://www.matrixscience.com).
f) Spearman's correlation.
g) Wilcoxon test.

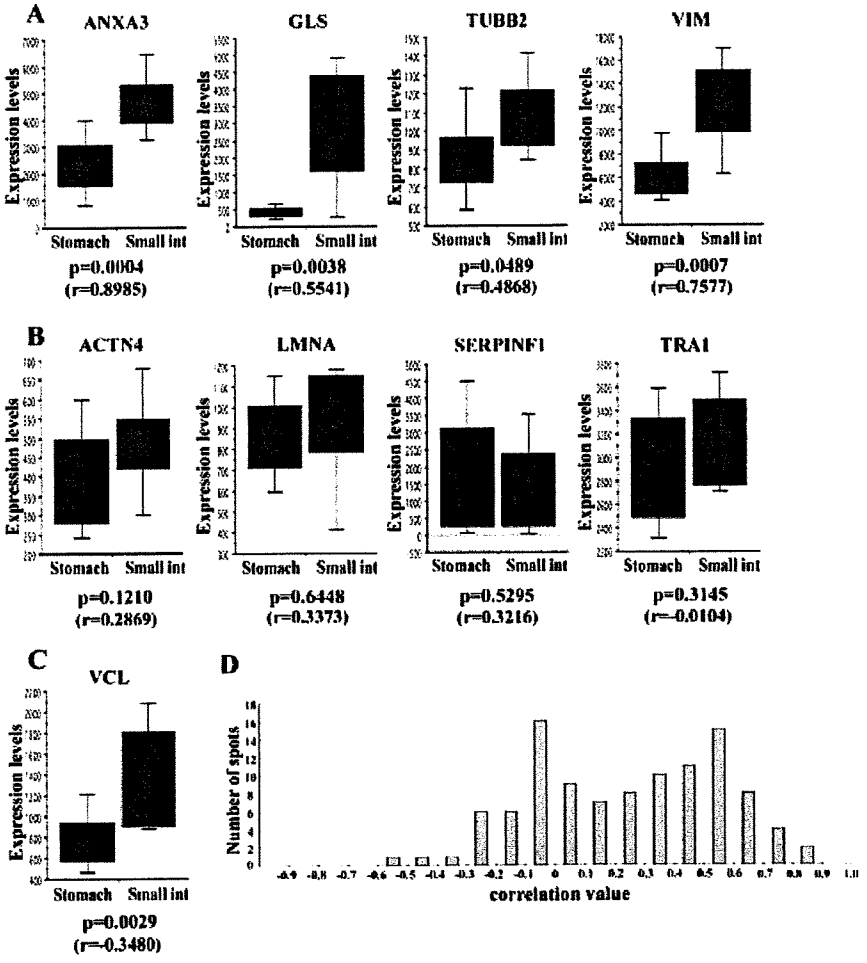

Figure 2. (A-C) A detailed comparison between mRNA and protein level is demonstrated for nine gene products that generated multiple protein spots. (A) The mRNA expression levels of annexin A3, glutaminase kidney isoform, tubulin beta-2 chain and vimentin. These genes showed different expression at the mRNA level between the gastric and small intestinal GIST (p <0.01). (B) The mRNA expression levels of alpha-actinin 4, lamin A/C, pigment epithelium-derived factor, and endoplasmin were not significantly different between the gastric and small intestinal GIST (p >0.01). (C) The mRNA expression level of vinculin. Vinculin showed significantly increased expression in the small intestinal GIST at the mRNA level (p <0.01), while vinculin expression was significantly lower in the small intestine (p <0.01). The correlation between mRNA and protein level of these genes is demonstrated by the r-value shown under the panels. (D) Among the 105 protein spots examined, only 37 showed significant correlation in intensity with mRNA expression (r >0.449, p <0.01).

at the protein level and only a limited number of proteins may have a key role in the tumors exhibiting varying clinical behavior. Indeed, the overall features of the proteome were not distinct between the intestinal and gastric tumors (Supporting Information Fig. 1). Secondly, as indicated by the number of protein spots observed in this study, 2-D DIGE uncovers only a limited portion of the proteome, which includes the proteins that are different between the two GIST types, and further improvement of the performance of 2-D DIGE will result in the identification of proteins with larger fold differences between the groups and lower expression levels.

Among the proteins identified by mass spectrometry (Fig. 1A), we found that the expression of several proteins known to be crucial to cancer development correlated with the anatomical site. One of the protein spots corresponding to prohibitin showed decreased intensity in intestinal GIST. Prohibitin has an antiproliferative activity by inhibiting DNA synthesis [16], and is down-regulated in stomach cancer [17, 18]. Similarly, the intensity of two protein spots corresponding to the pigment epithelium-derived factor (PEDF) was lower in the intestinal GIST. PEDF is neurotrophic[19] and has multifunctional antitumor activity by inhibiting the growth of tumor cells and angiogenesis[20–22]. The lower levels of PEDF have been associated with significantly poorer clinical outcome in lung cancer [23], breast cancer [24], pancreatic cancer [25], and lymphangioma [26]. These reports and our observations suggest that the decreased expression of PEDF may be associated with poor prognosis in small intestinal GIST. PEDF has been considered as a therapeutic tool in preclinical studies of ovarian cancer [27], pancreatic cancer [28], osteosarcoma [29, 30], neuroblastoma [31], melanoma [32], and liver cancer [33], suggesting that it may be similarly applied to GIST. The intensity of three alpha actinin-4 spots increased in the intestinal GIST. Alpha actinin-4 plays a key role in tumor invasion and cell motility, and aberrant expression of alpha-actinin 4 has been reported in a variety of malignancies, including prostate [34], esophageal [35], colorectal [36], lung [37, 38] and breast cancer [39]. Therefore, our proteomic study revealed a novel association

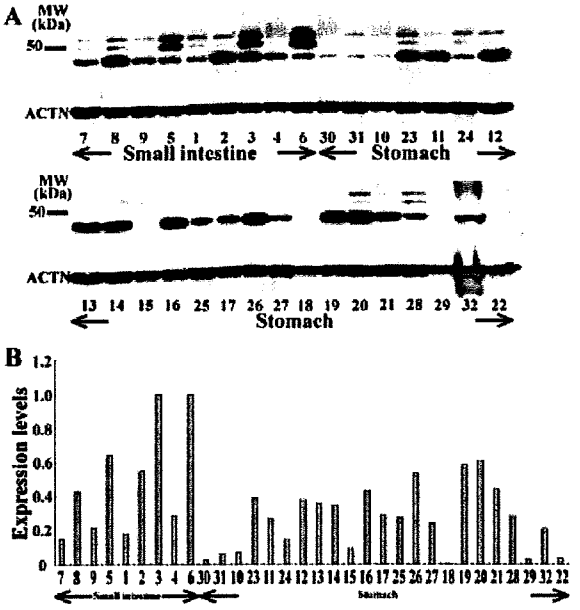

Figure 3. Western blotting for vimentin. (A) Vimentin expression was monitored by Western blotting. The upper and lower panels indicate the signals for vimentin and actin, respectively. (B) The whole intensity was measured and plotted in bar graph. Expression level was calculated by standardizing a sum of the intensity of multiple vimentin bands by the intensity of actin bands of the identical membrane.

of a number of genes, previously reported to be aberrantly expressed in a range of other malignancies, with small intestinal GIST. These observations indicate that the propensity of small intestinal GIST to exhibit malignant behavior may be attributable to the general, rather than tumor-type specific, mechanisms leading to malignant behavior of tumor cells. Subsequent studies that will examine the direct correlation between the identified proteins and survival may clarify their prognostic value. Biological validation of the contribution of these proteins to the poor prognosis of patients with the small intestinal GIST will also be worth considering, using cell lines and animal models.

In our sample set, the frequency of c-kit mutations at exons 9 and 11 was significantly high in the small intestinal and gastric GIST, respectively (Table 1). A correlation between the type of c-kit mutations and the anatomical site has also been reported in previous studies [8, 40]. Therefore, the proteomic differences observed between gastric and small intestinal GIST may include differences that are due to genotype differences. As the presence of c-kit mutations is one of the major prognostic factors for GIST cases, the molecular mechanisms underlying the differences in the behavior of GIST subtypes associated with the type of KIT mutations present is of significant interest.

We observed a significant level of discordance between the spot intensity in 2-D DIGE and the mRNA level as detected using a DNA microarray (Fig. 2). This discordance, when present, does not necessarily mean that the actual expression of identical genes at the mRNA and protein level is discordant. The intensity of each spot represents the expression level of a single isoform, and a sum of the intensity values of individual spots for a certain gene presumably represents the total amount of the expressed protein. In this study, the protein spots the intensity of which was not statistically different between the gastric and small intestinal GIST were not subjected to mass spectrometric protein identification, and there may be protein spots corresponding to isoforms other than the ones identified. The fact that the mRNA and protein expression levels were not consistently concordant may be partially due to the presence of such isoforms. The discrepancy between the 2-D DIGE and Western blotting results may also be attributable to the presence of protein spots whose intensity was unchanged or inversely changed between the two sample groups. Each isoform should have a distinct function, and only one of the isoforms may be a biomarker candidate. The 2-D DIGE is a technology with superior resolution separation that allows the identification of a change of even a small population of proteins, a attribute not shared by the other conventional separation methods. However, this high resolution may at the same time limit the application for biomarker identification. We found that 18 of the 105 identified protein spots corresponded to vimentin, and 17 of 18 showed higher intensity in the small intestinal GIST samples. However, the total amount of vimentin, as measured by Western blotting, did not show significant differences between the gastric and small intestinal GIST. Furthermore, we found two bands with slower migration in the small intestinal GIST samples; as they were specific to this group, their expression is worth being examined in additional samples. These results may suggest that specific probes against specific isoform spots or bands will be required to examine the isoforms identified by 2-D DIGE using routine clinical techniques such as ELISA and immunohistochemistry. Alternatively, we may be able to construct an easy to operate, automatic, robust, cost-effective electrophoresis and western blotting device. Both approaches will be a major challenge as a next step for biomarker development by 2-D DIGE. Although GIST are the most common primary mesenchymal tumors of the digestive tract, their prevalence is limited to 15–20 *per* 1 000 000 [1, 2], limiting the number of GIST samples available for proteomic studies. Further validation studies using an adequate number of samples will need to be performed, through the collaboration between multiple institutes, to clarify the prognostic utility or otherwise of the identified proteins. We consider that the clinical application of biomarkers identified by proteomics will need to rely on the use of practical tools such as ELISA and immunohistochemistry rather than 2-D DIGE.

In this study, we did not observe gene products previously reported to be associated with GIST such as c-kit and connexin 43 [8], a fact that possibly suggests that the sensitivity of 2-D DIGE technology should be further improved in

order to comprehensively understand the proteomic aberrations of malignant tumors. We have developed an easily operated large format electrophoresis apparatus that generates 5000 protein spots, and the application of laser microdissection for accurate sampling, as well as an effective in-gel digestion protocol for protein identification [41, 42]. Continuing efforts for increasingly more comprehensive proteomics will further our understanding of cancer biology, identify crucial proteins for diagnosis and therapy, and finally benefit cancer patients.

This study was supported by the Program for Promotion of Fundamental Studies in Health Sciences of the National Institute of Biomedical Innovation of Japan, a grant-in-aid for the Third-Term Comprehensive 10-year Strategy for Cancer Control from the Ministry of Health, Labor and Wealth of Japan and a grant-in-aid for Young Scientists (start-up) No. 20890218 from the Japan Society for the Promotion of Science.

The authors have declared no conflict of interest.

5 References

[1] Joensuu, H., Kindblom, L. G., Gastrointestinal stromal tumors–a review. *Acta Orthop. Scand. Suppl.* 2004, *75*, 62–71.

[2] Miettinen, M., El-Rifai, W., L, H. L. S., Lasota, J., Evaluation of malignancy and prognosis of gastrointestinal stromal tumors: a review. *Hum. Pathol.* 2002, *33*, 478–483.

[3] Suehara, Y., Kondo, T., Seki, K., Shibata, T. *et al.*, Pfetin as a prognostic biomarker of gastrointestinal stromal tumors revealed by proteomics. *Clin. Cancer Res.* 2008, *14*, 1707–1717.

[4] Emory, T. S., Sobin, L. H., Lukes, L., Lee, D. H., O'Leary, T. J., Prognosis of gastrointestinal smooth-muscle (stromal) tumors: dependence on anatomic site. *Am. J. Surg. Pathol.* 1999, *23*, 82–87.

[5] Fletcher, C. D., Berman, J. J., Corless, C., Gorstein, F. *et al.*, Diagnosis of gastrointestinal stromal tumors: a consensus approach. *Int. J. Surg. Pathol.* 2002, *10*, 81–89.

[6] Wozniak, A., Sciot, R., Guillou, L., Pauwels, P. *et al.*, Array CGH analysis in primary gastrointestinal stromal tumors: cytogenetic profile correlates with anatomic site and tumor aggressiveness, irrespective of mutational status. *Genes Chromosomes Cancer* 2007, *46*, 261–276.

[7] Antonescu, C. R., Viale, A., Sarran, L., Tschernyavsky, S. J. *et al.*, Gene expression in gastrointestinal stromal tumors is distinguished by KIT genotype and anatomic site. *Clin. Cancer Res.* 2004, *10*, 3282–3290.

[8] Nishitani, A., Hirota, S., Nishida, T., Isozaki, K. *et al.*, Differential expression of connexin 43 in gastrointestinal stromal tumours of gastric and small intestinal origin. *J. Pathol.* 2005, *206*, 377–382.

[9] Agaram, N., Wong, G., Guo, T., Maki, R. *et al.*, Novel V600E BRAF mutations in imatinib-naive and imatinib-resistant gastrointestinal stromal tumors. *Genes Chromosomes Cancer* 2008, *47*, 853–859.

[10] Braconi, C., Bracci, R., Bearzi, I., Bianchi, F. *et al.*, Insulin-like growth factor (IGF) 1 and 2 help to predict disease outcome in GIST patients. *Ann. Oncol.* 2008, *19*, 1293–1298.

[11] Stankey RH, L. A., *Pathology and Genetics of Tumours of the Digestive System*, IARC Press, Lyon 2000.

[12] Hasegawa, T., Matsuno, Y., Shimoda, T., Hirohashi, S., Gastrointestinal stromal tumor: consistent CD117 immunostaining for diagnosis, and prognostic classification based on tumor size and MIB-1 grade. *Hum. Pathol.* 2002, *33*, 669–676.

[13] Antonescu, C. R., Sommer, G., Sarran, L., Tschernyavsky, S. J. *et al.*, Association of KIT exon 9 mutations with nongastric primary site and aggressive behavior: KIT mutation analysis and clinical correlates of 120 gastrointestinal stromal tumors. *Clin. Cancer Res.* 2003, *9*, 3329–3337.

[14] Lasota, J., Jasinski, M., Sarlomo-Rikala, M., Miettinen, M., Mutations in exon 11 of c-Kit occur preferentially in malignant versus benign gastrointestinal stromal tumors and do not occur in leiomyomas or leiomyosarcomas. *Am. J. Pathol.* 1999, *154*, 53–60.

[15] Lasota, J., Dansonka-Mieszkowska, A., Stachura, T., Schneider-Stock, R. *et al.*, Gastrointestinal stromal tumors with internal tandem duplications in 3′ end of KIT juxtamembrane domain occur predominantly in stomach and generally seem to have a favorable course. *Mod. Pathol.* 2003, *16*, 1257–1264.

[16] Nuell, M. J., Stewart, D. A., Walker, L., Friedman, V. *et al.*, Prohibitin, an evolutionarily conserved intracellular protein that blocks DNA synthesis in normal fibroblasts and HeLa cells. *Mol. Cell. Biol.* 1991, *11*, 1372–1381.

[17] Jang, J. S., Cho, H. Y., Lee, Y. J., Ha, W. S., Kim, H. W., The differential proteome profile of stomach cancer: identification of the biomarker candidates. *Oncol. Res.* 2004, *14*, 491–499.

[18] He, Q. Y., Cheung, Y. H., Leung, S. Y., Yuen, S. T. *et al.*, Diverse proteomic alterations in gastric adenocarcinoma. *Proteomics* 2004, *4*, 3276–3287.

[19] Steele, F. R., Chader, G. J., Johnson, L. V., Tombran-Tink, J., Pigment epithelium-derived factor: neurotrophic activity and identification as a member of the serine protease inhibitor gene family. *Proc. Natl. Acad. Sci. USA* 1993, *90*, 1526–1530.

[20] Dawson, D. W., Volpert, O. V., Gillis, P., Crawford, S. E. *et al.*, Pigment epithelium-derived factor: a potent inhibitor of angiogenesis. *Science* 1999, *285*, 245–248.

[21] Maik-Rachline, G., Shaltiel, S., Seger, R., Extracellular phosphorylation converts pigment epithelium-derived factor from a neurotrophic to an antiangiogenic factor. *Blood* 2005, *105*, 670–678.

[22] Doll, J. A., Stellmach, V. M., Bouck, N. P., Bergh, A. R. *et al.*, Pigment epithelium-derived factor regulates the vasculature and mass of the prostate and pancreas. *Nat. Med.* 2003, *9*, 774–780.

[23] Zhang, L., Chen, J., Ke, Y., Mansel, R. E., Jiang, W. G., Expression of pigment epithelial derived factor is reduced in non-small cell lung cancer and is linked to clinical outcome. *Int. J. Mol. Med.* 2006, *17*, 937–944.

[24] Cai, J., Parr, C., Watkins, G., Jiang, W. G., Boulton, M., Decreased pigment epithelium-derived factor expression in

human breast cancer progression. *Clin. Cancer Res.* 2006, *12*, 3510–3517.

[25] Uehara, H., Miyamoto, M., Kato, K., Ebihara, Y. *et al.*, Expression of pigment epithelium-derived factor decreases liver metastasis and correlates with favorable prognosis for patients with ductal pancreatic adenocarcinoma. *Cancer Res.* 2004, *64*, 3533–3537.

[26] Sidle, D. M., Maddalozzo, J., Meier, J. D., Cornwell, M. *et al.*, Altered pigment epithelium-derived factor and vascular endothelial growth factor levels in lymphangioma pathogenesis and clinical recurrence. *Arch. Otolaryngol. Head Neck Surg.* 2005, *131*, 990–995.

[27] Cheung, L. W., Au, S. C., Cheung, A. N., Ngan, H. Y. *et al.*, Pigment epithelium-derived factor is estrogen sensitive and inhibits the growth of human ovarian cancer and ovarian surface epithelial cells. *Endocrinology* 2006, *147*, 4179–4191.

[28] Hase, R., Miyamoto, M., Uehara, H., Kadoya, M. *et al.*, Pigment epithelium-derived factor gene therapy inhibits human pancreatic cancer in mice. *Clin. Cancer Res.* 2005, *11*, 8737–8744.

[29] Ek, E. T., Dass, C. R., Contreras, K. G., Choong, P. F.,Pigment epithelium-derived factor overexpression inhibits orthotopic osteosarcoma growth, angiogenesis and metastasis. *Cancer Gene Ther.* 2007.

[30] Ek, E. T., Dass, C. R., Contreras, K. G., Choong, P. F., Inhibition of orthotopic osteosarcoma growth and metastasis by multitargeted antitumor activities of pigment epithelium-derived factor. *Clin. Exp. Metastasis* 2007, *24*, 93–106.

[31] Streck, C. J., Zhang, Y., Zhou, J., Ng, C. *et al.*, Adeno-associated virus vector-mediated delivery of pigment epithelium-derived factor restricts neuroblastoma angiogenesis and growth. *J. Pediatr. Surg.* 2005, *40*, 236–243.

[32] Garcia, M., Fernandez-Garcia, N. I., Rivas, V., Carretero, M. *et al.*, Inhibition of xenografted human melanoma growth and prevention of metastasis development by dual antiangiogenic/antitumor activities of pigment epithelium-derived factor. *Cancer Res.* 2004, *64*, 5632–5642.

[33] Matsumoto, K., Ishikawa, H., Nishimura, D., Hamasaki, K. *et al.*, Antiangiogenic property of pigment epithelium-derived factor in hepatocellular carcinoma. *Hepatology* 2004, *40*, 252–259.

[34] Hara, T., Honda, K., Shitashige, M., Ono, M. *et al.*, Mass spectrometry analysis of the native protein complex containing actinin-4 in prostate cancer cells. *Mol. Cell. Proteomics* 2007, *6*, 479–491.

[35] Hatakeyama, H., Kondo, T., Fujii, K., Nakanishi, Y. *et al.*, Protein clusters associated with carcinogenesis, histological differentiation and nodal metastasis in esophageal cancer. *Proteomics* 2006, *6*, 6300–6316.

[36] Honda, K., Yamada, T., Hayashida, Y., Idogawa, M. *et al.*, Actinin-4 increases cell motility and promotes lymph node metastasis of colorectal cancer. *Gastroenterology* 2005, *128*, 51–62.

[37] Yamagata, N., Shyr, Y., Yanagisawa, K., Edgerton, M. *et al.*, A training-testing approach to the molecular classification of resected non-small cell lung cancer. *Clin. Cancer Res.* 2003, *9*, 4695–4704.

[38] Menez, J., Le Maux Chansac, B., Dorothee, G., Vergnon, I. *et al.*, Mutant alpha-actinin-4 promotes tumorigenicity and regulates cell motility of a human lung carcinoma. *Oncogene* 2004, *23*, 2630–2639.

[39] Honda, K., Yamada, T., Endo, R., Ino, Y. *et al.*, Actinin-4, a novel actin-bundling protein associated with cell motility and cancer invasion. *J. Cell. Biol.* 1998, *140*, 1383–1393.

[40] Corless, C. L., Fletcher, J. A., Heinrich, M. C., Biology of gastrointestinal stromal tumors. *J. Clin. Oncol.* 2004, *22*, 3813–3825.

[41] Kondo, T., Seike, M., Mori, Y., Fujii, K. *et al.*, Application of sensitive fluorescent dyes in linkage of laser microdissection and two-dimensional gel electrophoresis as a cancer proteomic study tool. *Proteomics* 2003, *3*, 1758–1766.

[42] Kondo, T., Hirohashi, S., Application of highly sensitive fluorescent dyes (CyDye DIGE Fluor saturation dyes) to laser microdissection and two-dimensional difference gel electrophoresis (2-D DIGE) for cancer proteomics. *Nat. Protoc.* 2007, *1*, 2940–2956.

RESEARCH ARTICLE

GST-P1 as a histological biomarker of synovial sarcoma revealed by proteomics

Yoshiyuki Suehara[1, 2, 3], Kazutaka Kikuta[1, 3, 4], Robert Nakayama[4, 5], Naobumi Tochigi[6], Kunihiko Seki[6], Hitoshi Ichikawa[5], Kiyonaga Fujii[1]**, Tadashi Hasegawa[6]***, Tadakazu Shimoda[6], Hisashi Kurosawa[2], Hirokazu Chuman[3], Yasuo Beppu[3], Akira Kawai[3], Setsuo Hirohashi[1] and Tadashi Kondo[1]*

[1] Proteome Bioinformatics Project, National Cancer Center Research Institute, Tokyo, Japan
[2] Department of Orthopedic Surgery, Juntendo University School of Medicine, Juntendo, Japan
[3] Orthopedic Surgery Division, National Cancer Center Hospital, Tokyo, Japan
[4] Department of Orthopedic Surgery, Keio University, Keio, Japan
[5] Cancer Transcriptome Project, National Cancer Center Research Institute, Tokyo, Japan
[6] Pathology Division, National Cancer Center Research Institute, Tokyo, Japan
[7] Clinical Laboratory Division, National Cancer Center Hospital, Tokyo, Japan

Received: October 18, 2008
Revised: November 29, 2008
Accepted: December 2, 2008

Synovial sarcoma have two histological subtypes, biphasic and monophasic, defined respectively by the presence or absence of glandular epithelial differentiation. To develop histological biomarkers for synovial sarcoma subtypes, we examined the proteomic profile using two-dimensional difference gel electrophoresis. We identified 29 protein spots whose intensity was statistically different between the monophasic (15 cases) and biphasic (9 cases) subtypes ($p < 0.01$). Mass spectrometric protein identification demonstrated that these 29 spots corresponded to 24 distinct gene products involved in cytoskeletal organization, trsnscription/trsnslation, protein/collagen binding, and ion transport, as well as structural constituents of the epidermis. Two of the 29 spots derived from glutathione S-transferase P (GST-P1) had higher intensity in biphasic type. Immunohistochemistry on additional 42 synovial sarcoma cases revealed that positive expression of GST-P1 was observed in 10 of 12 biphasic (83.3%), in 4 of 27 monophasic (14.8%) and in 1 of 3 poorly differentiated synovial sarcomas ($p = 0.0002$). Among the clinico-pathological parameters examined, GST-P1 expression significantly correlated only with the histological subtype. GST-P1 had more discriminative power than the status of fusion genes SYT-SSX1 and SYT-SSX2, previously reported to be correlated with the histological subtype. These results establish GST-P1 as a histological biomarker candidate for synovial sarcoma differentiation into subtypes.

Keywords:
2-D DIGE / GST-P1 / Proteomics / Synovial sarcoma

1 Introduction

Synovial sarcoma accounts for 5–10% of soft tissue sarcomas and is primarily located in the extremities, most frequently affecting young adults. At present, the 5-year survival rate for synovial sarcoma patients is approximately 60% [1–4]. Histologically, there are two major morphological forms of synovial sarcoma; the biphasic subtype, composed of epithelial and spindle tumor cells, and the monophasic subtype, composed solely of spindle tumor cells [1]. The molecular

Correspondence: Dr. Tadashi Kondo, Proteome Bioinformatics Project, National Cancer Center Research Institute, 5-1-1 Tsukiji, Chuo-ku, Tokyo 104-0045, Japan
E-mail: takondo@ncc.go.jp
Fax: +81-3-3547-5298

* Present address: Department of Pathology, JR Tokyo General Hospital, Tokyo, Japan
** Present address: Department of Structural Biology, Graduate School of Pharmaceutical Sciences, Hokkaido University, Hokkaido, Japan
*** Present address: Department of Surgical Pathology, Sapporo Medical University School of Medicine, Sapporo, Japan

background of synovial sarcoma has been extensively studied to predict the behavior of individual tumors. Synovial sarcomas are characterized by a t(X;18)(p11.2;11.2) fusion, representing the fusion of the SYT gene with either SSX1 or SSX2 [5–8]. Data from clinical samples suggested a link between the type of SYT-SSX protein fusion and the potential for epithelial differentiation; the SYT-SSX1 transcript was found in both monophasic and biphasic tumors, whereas almost all tumors with the SYT-SSX2 transcript were monophasic [9–11]. However, these findings have not been confirmed and were inconsistent in other reports [12, 13]. The differentiation lineage of synovial sarcoma is unclear, and in addition to potential clinical relevance, the regulation of epithelial differentiation in these tumors is a biological issue of interest.

Recent comprehensive studies offered a global view of molecular aberrations associated with the malignant spectrum of synovial sarcoma [14, 15]. Global mRNA expression studies using DNA microarrays identified the genes that are involved in the signaling pathways specific to the cellular origin of synovial sarcoma, the genes associated with histological features denoting malignancy, and the genes differentially expressed corresponding to the different histological subtypes and fusion genes [14, 15]. These comprehensive studies improved our understanding of the biology of synovial sarcoma and may lead to the development of practical tumor markers to support individualized therapy. Emerging technologies that examine the overall features of the expressed proteins, namely the proteome, have identified many candidate proteins associated with early diagnosis [16], differential diagnosis [17], prognosis [18, 19], and response to chemotherapy in various diseases [20] but have not been employed in the study of synovial sarcoma until now.

In this report, we performed a proteomics study on synovial sarcoma clinical samples using 2-D DIGE and MS. We found that the expression levels of 29 protein spots had different intensity corresponding to different histological subtypes. These spots included two variants of GST-P1 (glutathione S-transferase P), a protein the high expression of which has been originally reported to be related to epithelial differentiation [21, 22], drug resistance [22–26] and carcinogenesis [23, 27–34] in malignant tumors other than synovial sarcoma. We verified the expression of GST-P1 in 42 synovial sarcoma cases using immunohistochemistry, and found that it was significantly different between the biphasic and monophasic synovial sarcomas. These results establish GST-P1 as a biomarker for synovial sarcoma differentiation into histological subtypes. GST-P1 may play an important role in the potential for epithelial differentiation of synovial sarcoma.

2 Materials and methods

2.1 Patients and clinical information

We examined the tumor tissues of 49 synovial sarcoma patients who underwent surgery or chemotherapy at the National Cancer Center Hospital consecutively from February 1995 to August 2004. Histological features of the tissues were reviewed by three board-certified pathologists (K. S., T. H., and N. T). Diagnosis and classification was based on the WHO classification system for soft-tissue tumors [1], and included the examination of *SYT-SSX1* and *SYT-SSX2* expression. This project was approved by the institutional review board of the National Cancer Center. Frozen tumor tissues were used for the proteomic analysis, and were available in 28 of 49 cases, including 15 monophasic, 9 biphasic, and 4 poorly differentiated synovial sarcomas. Immunohistochemistry was performed on 42 of 49 cases, consisting of 27 monophasic, 12 biphasic, and 3 poorly differentiated synovial sarcomas. The clinical data pertaining to the cases examined are summarized in Table 1 and Supporting Information Table 1.

2.2 Protein expression profiling

The frozen samples were crushed to powder with a Cryo-Press (Microtech Nichion, Chiba, Japan) under cooling with liquid nitrogen. The frozen powder was then treated with urea lysis buffer (6 M urea, 2 M thiourea, 3% CHAPS, 1% Triton X-100). After centrifugation at 15 000 rpm for 30 min, the supernatant was used as the source of cellular proteins for protein expression studies.

The 2-D DIGE was performed as described previously [17, 18, 20, 35]. In brief, the internal control sample was prepared by mixing a portion of all individual samples. Five micrograms each of the internal control sample and of each individual sample were labeled with Cy3 and Cy5 respectively (CyDye DIGE Fluor saturation dye, GE Healthcare Biosciences, Uppsala, Sweden). The differently labeled protein samples were mixed and then separated, by IPG DryStrip gels for the first dimension separation (24-cm length, p*I* range 4–7, GE Healthcare Biosciences) and then by SDS-PAGE for the second dimension separation (EttanDalt II, GE Healthcare Biosciences). The gels were scanned using laser scanners (Tyhoon Trio, GE Healthcare Biosciences) at the appropriate wavelengths (Fig. 1A and Supporting Information Fig. 1). For all spots, the intensity of the Cy5 image was normalized by that of the Cy3 image from the same gel so that gel-to-gel differences were compensated, using the DeCyder image software (GE Healthcare Biosciences). System reproducibility was verified by comparing the protein profiles obtained from three independent separations of the same sample (sample 22, Table 1 and Supporting Information Table 1). Scatter plot analysis revealed that the standardized intensity of more than 96% of the spots ranged within a twofold difference (Fig. 1B). Representative 2-D images with the numbers of the identified spots are shown in Fig. 1A and Supporting Information Fig. 1.

2.3 Data analysis

The protein spots whose intensity was statistically different between the groups examined were identified using the

Table 1. Clinicopathological features of synovial sarcoma samples (28 cases)

Sample no.	Histological subtype	Age	Gender	Primary location	Fusion gene
1	Monophasic	60	M	Forearm	SYT/SSX2
2	Monophasic	29	M	Shoulder	SYT/SSX1
3	Monophasic	37	M	Shoulder	SYT/SSX1
4	Monophasic	21	M	Knee	SYT/SSX1
5	Monophasic	33	F	Foot	SYT/SSX2
6	Monophasic	17	M	Neck	not detect
7	Monophasic	57	F	Knee	SYT/SSX1
8	Monophasic	30	F	Thigh	SYT/SSX1
9	Monophasic	14	M	Foot	SYT/SSX1
10	Monophasic	26	M	Lower leg	SYT/SSX2
11	Monophasic	41	M	Upper arm	SYT/SSX1
12	Monophasic	40	M	Lower leg	SYT/SSX1
13	Monophasic	52	M	Hand	SYT/SSX1
14	Monophasic	56	F	Retroperitoneum	SYT/SSX1
15	Monophasic	17	F	Lower leg	SYT/SSX2
16	Biphasic	41	F	Thigh	SYT/SSX1
17	Biphasic	41	F	Foot	SYT/SSX1
18	Biphasic	51	M	Hand	SYT/SSX1
19	Biphasic	61	F	Thigh	SYT/SSX1
20	Biphasic	10	F	Elbow	SYT/SSX2
21	Biphasic	27	F	Abdominal wall	not detect
22	Biphasic	33	F	Inguen	SYT/SSX1
23	Biphasic	24	M	Elbow	not detect
24	Biphasic	49	F	Foot	SYT/SSX1
25	Poor	17	F	Thigh	SYT/SSX2
26	Poor	19	F	Thigh	SYT/SSX2
27	Poor	54	M	Inguen	SYT/SSX1
28	Poor	47	F	Thigh	SYT/SSX1

Wilcoxon test (statistical significance was set at $p < 0.01$). Hierarchical clustering, PCA, correlation matrix studies and spot ranking were performed using the Expressionist software (Genedata, Basel, Switzerland).

2.4 Protein identification by MS

Proteins corresponding to the spots of interest were identified by MS according to our previous report [17, 18, 20, 35]. The Cy5-labeled proteins separated by 2-D PAGE were recovered in gel plugs and digested with modified trypsin (Promega, Madison, WI). The trypsin digests were subjected to a Finnigan LTQ linear IT mass spectrometer (Thermo Electron, San Jose, CA) equipped with a nano-electrospray ion source (AMR, Tokyo, Japan). The MASCOT software (version 2.1, Matrix Science, London, UK) was used to search for the mass of the peptide ion peaks against the Swiss-Prot database (*Homo sapiens*, 12 867 sequences in Sprot_47.8 fasta file). A MASCOT score of 35 or more was considered as indicating positive protein identification. When multiple proteins were identified in a single spot, the proteins with the highest number of peptides were considered as those corresponding to the spot.

2.5 Western blotting and immunohistochemistry

Protein samples were separated by SDS-PAGE and subsequently blotted on an NC membrane. The membrane was incubated with a rabbit polyclonal antibody against GST-P1 (1:1000 dilution, MBL international corporation, Woburn, MA), and then HRP-conjugated secondary antibody (1:1000 dilution, GE Healthcare Biosciences). GST-P1 was detected using an enhanced chemiluminescence system (GE Healthcare Biosciences) and LA 3000 (Fuji Film, Tokyo, Japan).

GST-P1 expression was examined immunohistochemically using paraffin-embedded tissues. In brief, 4-μm-thick tissue sections were incubated with the antibody against GST-P1 (1:1000 dilution). Immunostaining was performed according to the streptavidin-biotin peroxidase method using the Strept ABC Complex/HRP kit (DAKO, Tokyo, Japan). Three investigators (Y.S., N.T. and K.S) reviewed the sections stained with the anti-GST-P1 antibody in a blinded fashion regarding clinical data (age, sex, anatomic site, and subtypes). The cases were considered as positive when more than 20% of tumor cells were stained.